

## Electrochemical Properties of $\text{Cu}_6\text{Sn}_5\text{-C}$ Composite Powders with Mixture of $\text{Cu}_5\text{Sn}_6@void@C$ Yolk-Shell, $\text{Cu}_5\text{Sn}_6$ Alloy, and Hollow Carbon

Yong Seung Jang, Jung Hyun Kim, Seung Ho Choi, Kwang Min Yang, Yun Chan Kang\*

Department of Chemical Engineering, Konkuk University, 1 Hwayang-dong, Gwangjin-gu, Seoul 143-701, Republic of Korea

\*E-mail: [yckang@konkuk.ac.kr](mailto:yckang@konkuk.ac.kr)

Received: 22 October 2012 / Accepted: 11 November 2012 / Published: 1 December 2012

---

$\text{SnO}_2\text{-CuO-C}$  composite powders consisting of hollow-structured particles are directly prepared using template-free spray pyrolysis. Reduction of the composite powders at  $1000^\circ\text{C}$  produces  $\text{Cu}_6\text{Sn}_5\text{-C}$  composite powders containing a mixture of  $\text{Cu}_5\text{Sn}_6@void@C$  yolk-shell,  $\text{Cu}_5\text{Sn}_6$  alloy, and hollow carbon particles. In the yolk-shell powder, mobile  $\text{Cu}_5\text{Sn}_6$  powder particle is located inside the hollow hard-carbon powder particle. The mean sizes of the  $\text{Cu}_5\text{Sn}_6$  alloy and carbon powders are 0.7 and 1.6  $\mu\text{m}$ , respectively. The submicron  $\text{Cu}_5\text{Sn}_6$  alloy powders are coated with a uniformly thin carbon layer. The initial charge and discharge capacities of the composite powders are 254 and 578  $\text{mAh g}^{-1}$ , respectively, at a high current density of 300  $\text{mA g}^{-1}$ . The charge capacity of the composite powders slightly increases with increasing number of cycles during the first three cycles. The maximum charge capacity of the composite powders is 300  $\text{mAh g}^{-1}$ . The charge capacity of the composite powders is 241  $\text{mAh g}^{-1}$  after 30 cycles, at which point the capacity retention is 80%. The unique particle structure and phase homogeneity improve the cycle properties of the composite alloy powders.

---

**Keywords:** alloy powder, anode materials, spray pyrolysis, composite powders

### 1. INTRODUCTION

Alloy powders containing particles of various sizes and morphologies have widely been studied for application as anode materials in Li secondary batteries because of their high specific gravimetric and volumetric capacities [1-14]. Sn-based intermetallic compounds ( $\text{Sn}_x\text{M}_y$ , M: inactive material) including Cu-Sn, Ni-Sn, Sb-Sn, and Fe-Sn alloy systems have previously been reported as promising electrode materials [5-10]. Among them, Cu-Sn is the most promising candidate for application as anodes in Li ion battery because of its low price, high conductivity, and good capacity retention.

The  $\text{Cu}_6\text{Sn}_5$  alloy of the Cu-Sn system has previously been prepared using various methods including high-energy ball milling, spray pyrolysis, chemical reduction in aqueous and nonaqueous solutions, and solid-state reaction [11-18]. The electrochemical properties of the Cu-Sn system alloys are strongly affected by the phase homogeneity of the powders. However, it is difficult to obtain pure  $\text{Cu}_6\text{Sn}_5$  phase alloy powders because of the various crystal structures within the Cu-Sn system. The nanosized Cu-Sn alloy powders synthesized using reductive precipitation of metal chlorides exhibited XRD peaks associated with  $\text{SnO}_2$  and copper-rich  $\text{Cu}_3\text{Sn}$  impurity phases [15,16]. The  $\text{Cu}_6\text{Sn}_5$  alloy powders prepared using spray pyrolysis at  $1100^\circ\text{C}$  also exhibited XRD peaks associated with the  $\text{Cu}_3\text{Sn}$  impurity phase [17]. The XRD patterns of the microspherical Cu-Sn alloy electrodeposited onto a porous Cu substrate exhibited peaks associated with a main  $\text{Cu}_6\text{Sn}_5$ -crystal-structured phase and those associated with minor phases of Sn, Cu, and unknown impurities [18].

The main disadvantage of using  $\text{Cu}_6\text{Sn}_5$  alloy electrodes for commercial applications is the large change in volume they exhibit during lithiation and delithiation. Enhancing their dimensional stability during cycling is a key factor for improving the cycle stability of  $\text{Cu}_6\text{Sn}_5$  alloy electrodes. Various types of particle structures such as core-shell and yolk-shell have previously been studied to improve the cycling performances of metal or alloy powders [15,16,19-24]. Amorphous carbon has widely been used as the shell material for covering active alloy powders [15,16,20-24]. Yolk-shell is a hollow particle structure consisting of a void space between the core and the shell, where the core particles are mobile inside the shell [23-25]. The shell material prevents powder aggregation during cycling.  $\text{Si@void@C}$  and  $\text{Sn@void@C}$  composite powders containing yolk-shell-structured particles have previously exhibited high capacities and excellent cycle properties [22-24]. The composite powders containing yolk-shell-structured particles were prepared using a complex multistep process with either organic or inorganic templates [25-32]. Therefore, multicomponent alloy composite powders containing yolk-shell-structured particles have rarely been studied.

Spray pyrolysis is thought to be an effective method of producing homogeneous composition alloy powders in a short residence time. The fine, spherical, densely structured alloy powders prepared using spray pyrolysis exhibited narrow size distribution [13,33,34]. In this study,  $\text{SnO}_2$ -CuO-C composite powders consisting of hollow particles were prepared directly using template-free spray pyrolysis. Reduction of the composite powders under a reducing atmosphere produced the  $\text{Cu}_6\text{Sn}_5$ -C composite powder particles exhibiting a unique morphology.

## 2. EXPERIMENTAL

The  $\text{SnO}_2$ -CuO-C composite powders were directly prepared using spray pyrolysis from a spray solution containing Sn, Cu, and C components. The spray pyrolysis system consisted of a droplet generator, a quartz reactor, and a powder collector. A 1.7-MHz ultrasonic spray generator with six vibrators was used to generate a large quantity of droplets, which were carried into the high-temperature tubular reactor by nitrogen carrier gas at a flow rate of  $10 \text{ L min}^{-1}$ . The droplets and powders evaporated, decomposed, and/or crystallized in the quartz reactor. The length and diameter of the quartz reactor were 1000 and 55 mm, respectively. The reactor temperature was fixed at  $900^\circ\text{C}$ .

The spray solution was prepared by dissolving a stoichiometric ratio of copper nitrate hydrate [ $\text{Cu}(\text{NO}_3)_2 \cdot 3\text{H}_2\text{O}$ , Aldrich] and stannic chloride hydrate [ $\text{SnCl}_2 \cdot 2\text{H}_2\text{O}$ , Aldrich] salts in distilled water. The overall solution concentration of the copper and tin components was 0.5 M. The concentration of the sucrose used as the carbon source was 0.5 M. The prepared composite powders were reduced at temperatures between 400 and 1000°C under a 10%  $\text{H}_2/\text{N}_2$  gas mixture to obtain the  $\text{Cu}_6\text{Sn}_5\text{-C}$  composite powders.

The crystal structures of the composite alloy powders were investigated using X-ray diffractometry (XRD, Rigaku DMAX-33) at the Korea Basic Science Institute (Daegu). The morphological characteristics of the composite powders were investigated using scanning electron microscopy (SEM, JEOL JSM-6060) and high-resolution transmission electron microscopy (HR-TEM, FEI Tecnai<sup>TM</sup> 300K). Measurement of the thermal properties of the composite powders was performed in a thermo-analyzer (TG-DSC, Mettler Toledo, TGA/SDTA 851e-DSC 823e) in the temperature range from 30 to 1000 °C (10 °C  $\text{min}^{-1}$ ).

The capacities and cycle properties of the composite alloy powders were measured using 2032-type coin cells. The electrodes were prepared by mixing 40 mg of composite powder, 5 mg of a carbon black, and 5 mg of sodium carboxymethyl cellulose (CMC) in distilled water. Li metal was used as the counter electrode, and polypropylene film was used as the separators. The electrolyte was 1 M  $\text{LiPF}_6$  mixed in a 1:1 volume ratio with ethylene carbonate/dimethyl carbonate (EC/DMC, Techno Semichem Co., Ltd., Korea). The entire cell was assembled in a glove box under an argon atmosphere. The charge/discharge characteristics of the samples were measured at room temperature at a constant current density of 300  $\text{mA g}^{-1}$  in the range 0.01–1.5 V.

### 3. RESULTS AND DISCUSSION

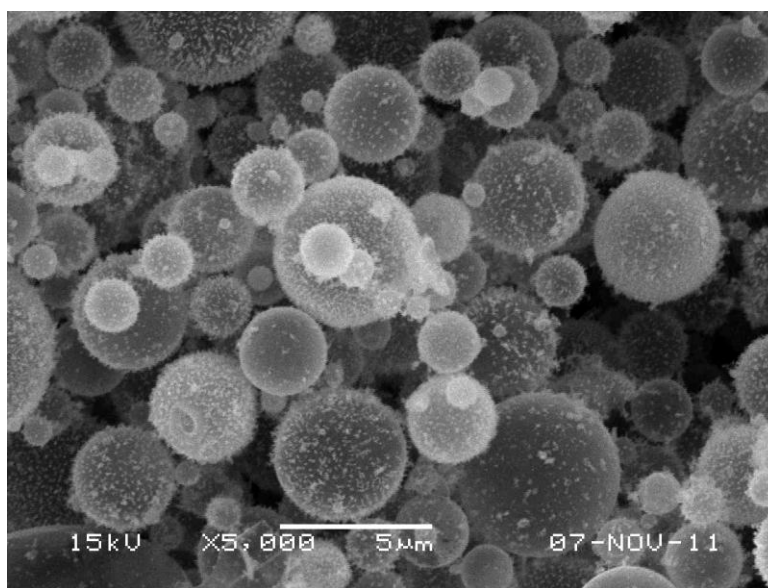


**Figure 1.** SEM image of the precursor powders prepared by spray pyrolysis.

The morphologies of the SnO<sub>2</sub>-CuO-C composite powders are shown in Fig. 1. The powder particles are hollow spheres that exhibit a thin-wall structure. Spherical carbon powder particles were formed from the decomposition of sucrose. Sudden gas evolution during the decomposition of sucrose and the precursors of the Sn and Cu components produced the hollow and spherical carbon powder particles. The Sn and Cu components became segregated during drying and decomposition of the droplets to form the composite particles. Nanosized SnO<sub>2</sub>-CuO composite particles were then uniformly dispersed over the inner and outer surfaces of the carbon powders. The mean size of the hollow SnO<sub>2</sub>-CuO-C composite powders, as measured from the SEM images, was 3 μm.

The composite powders were post-treated between 400 and 1000°C under a reducing atmosphere. The XRD patterns for the precursor and reduced powders are shown in Fig. 2.

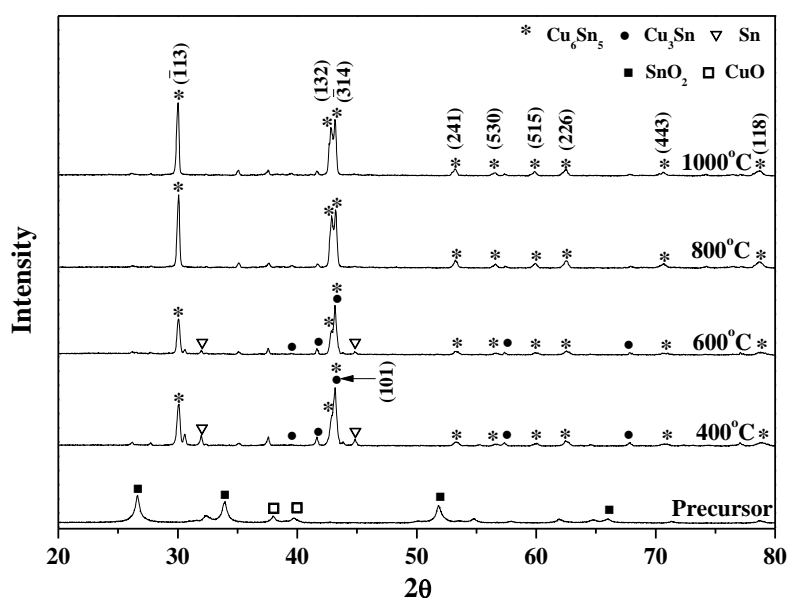
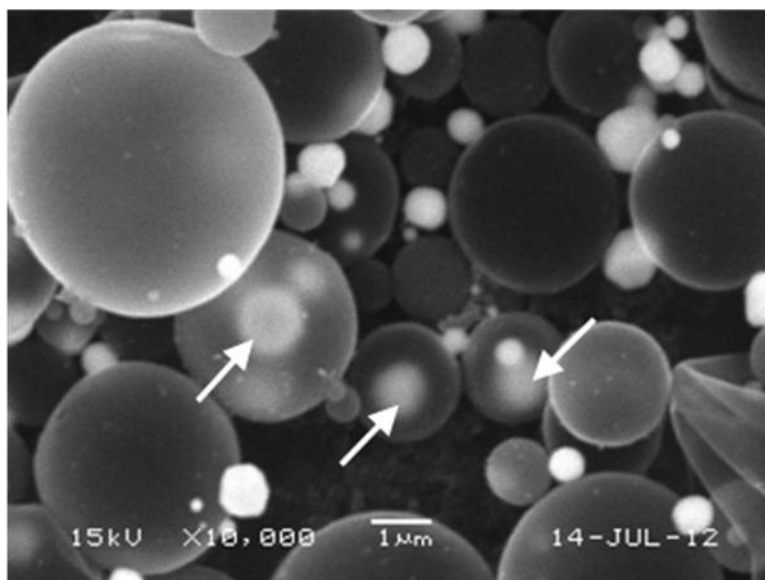


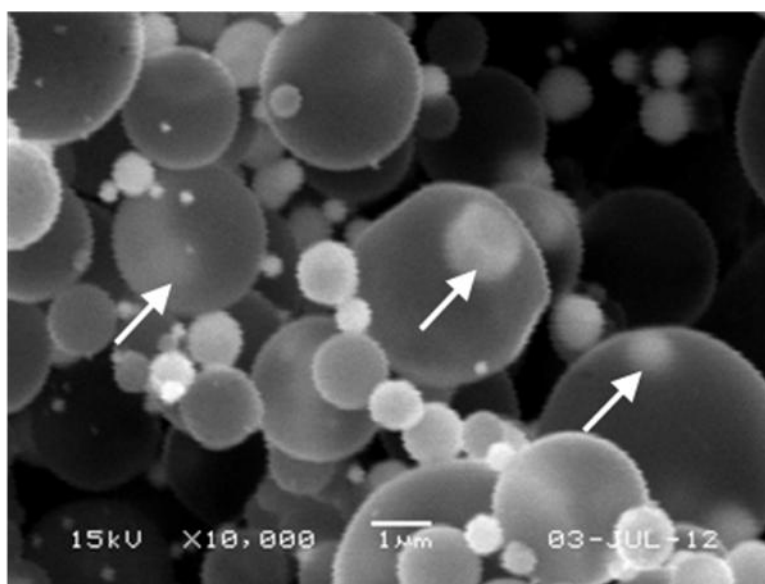
**Figure 2.** XRD patterns of the precursor and post-treated powders at various temperatures.

The patterns for the precursor powders exhibited low-intensity peaks associated with the SnO<sub>2</sub> and CuO mixed-crystal structure because of the short residence time the powder particles inside the hot-wall reactor. The XRD patterns for the composite powders reduced at 400°C exhibited peaks associated with the Cu<sub>3</sub>Sn, Cu<sub>6</sub>Sn<sub>5</sub>, Sn, and SnO<sub>2</sub> mixed crystal structure. The intensities of the (113) and (132) peaks associated with the Cu<sub>6</sub>Sn<sub>5</sub> phase increased with increasing reduction temperature. The (314) peak associated with the Cu<sub>6</sub>Sn<sub>5</sub> phase overlapped with the (101) peak associated with the Cu<sub>3</sub>Sn phase, and the intensity of the (314) peak increased with the increasing reduction temperature, corresponding to the growth in intensity of the (132) peak. The intensities of the (101) peak decreased with the increasing reduction temperature. The patterns for composite powders reduced at 800°C exhibited main peaks associated with the crystal structure of the Cu<sub>6</sub>Sn<sub>5</sub> phase. The intensity ratios of

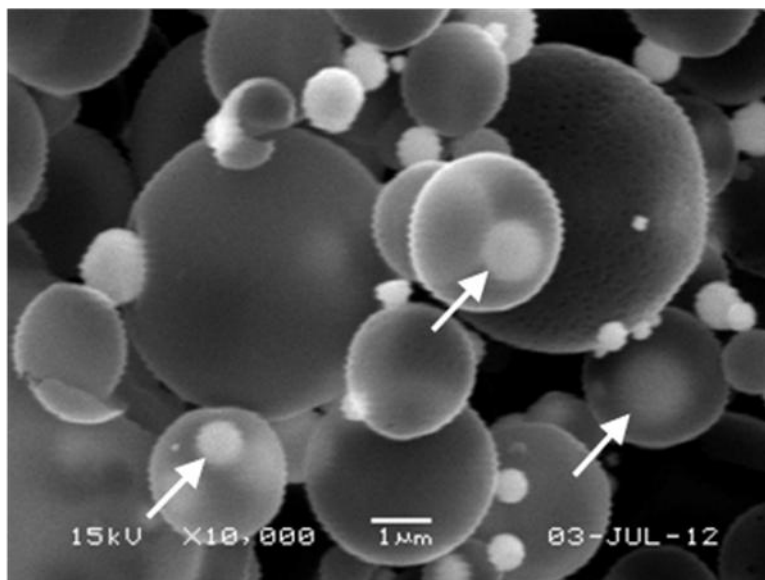
the  $(\bar{1},113)$  and  $(132)$  peaks for the composite powders reduced at 800 and 1000°C were consistent with those of  $\text{Cu}_6\text{Sn}_5$  (JCPDS card 45-1488). Peaks of negligible intensity associated with the  $\text{Cu}_3\text{Sn}$  and Sn impurity phases were observed in the XRD patterns for the composite powders reduced at 800 and 1000°C. In the previous report, pure  $\text{Cu}_6\text{Sn}_5$  phase powders could not be prepared using spray pyrolysis, even at a high temperature of 1300°C [17]. In this study, the carbon material of the composite powders decreased the reduction temperature of the Cu and Sn materials. The highly mixed Cu and Sn components of the precursor powders enabled the formation of the pure  $\text{Cu}_6\text{Sn}_5$  phase alloys at low reduction temperatures.



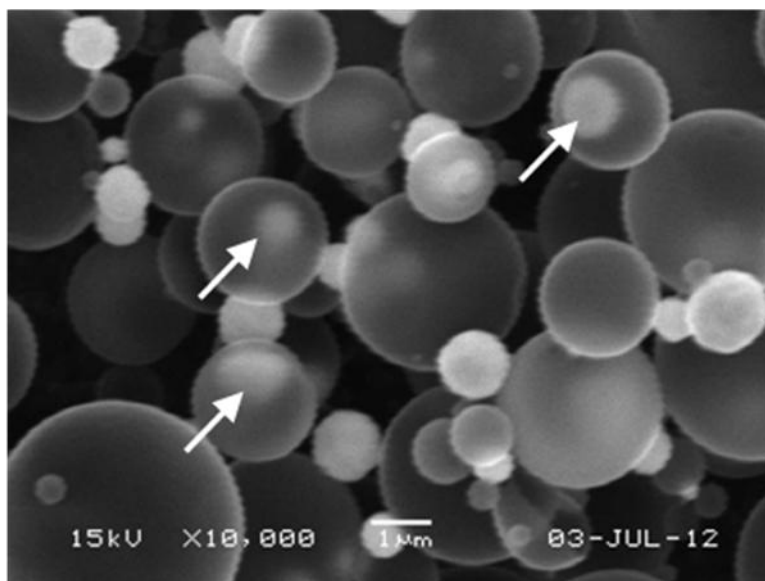
(a) 400°C



(b) 600°C



(c) 800°C

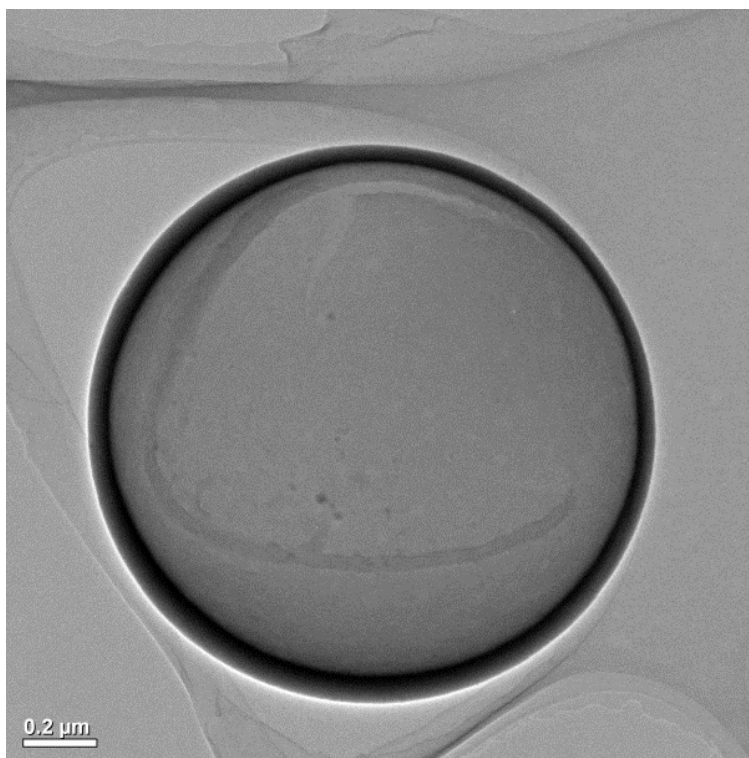


(d) 1000°C

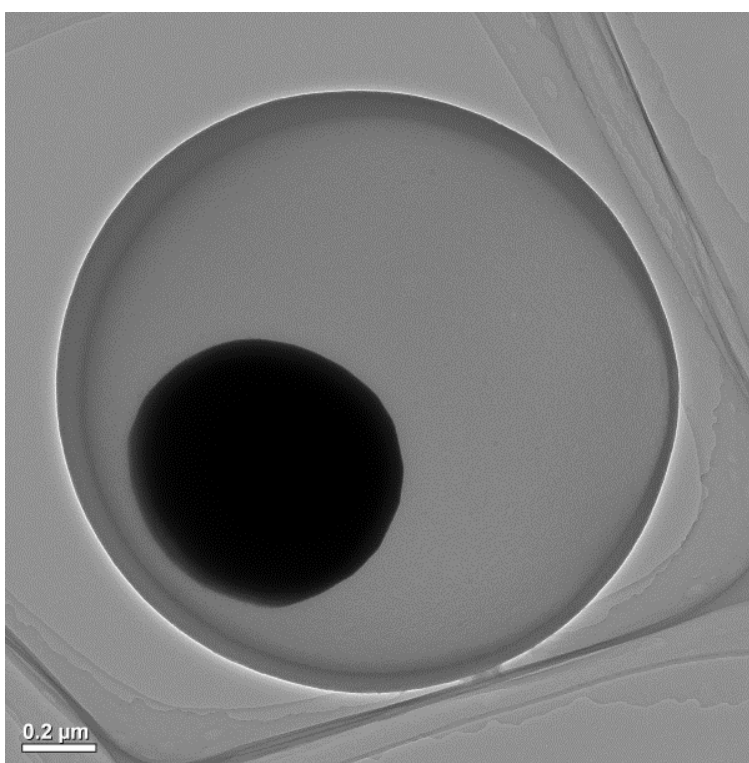
**Figure 3.** SEM image of the composite powders post-treated at various temperatures.

The particle morphologies of the Cu-Sn alloy powders reduced at various temperatures are shown in Figs. 3 and 4. The powders exhibited a bimodal distribution of submicron and microsized particles regardless of the reduction temperature. The formation mechanism of the alloy composite powders from the hollow SnO<sub>2</sub>-CuO-C composite powders is described in Fig. 5. The densely structured submicron Cu-Sn alloy particles were formed from the CuO-SnO<sub>2</sub> nanoparticles covering the composite powders. The Cu-Sn alloys had melted at low temperature and had grown into submicron particles during reduction. Some of the alloy powder particles had entered the interior of the

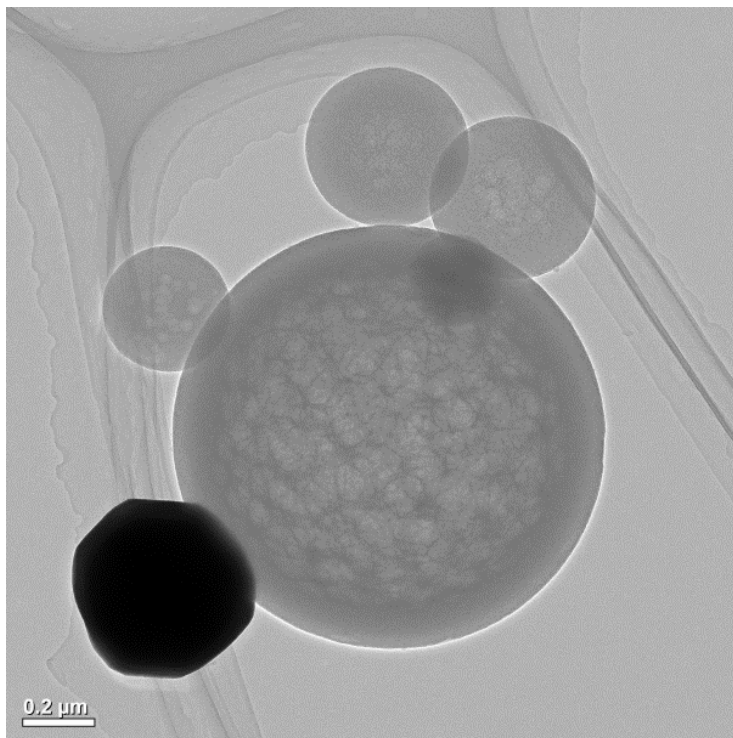
spherical carbon powder particles to form the  $\text{Cu}_5\text{Sn}_6@\text{void}@C$  yolk-shell powders, as shown by the arrows in Fig. 3.



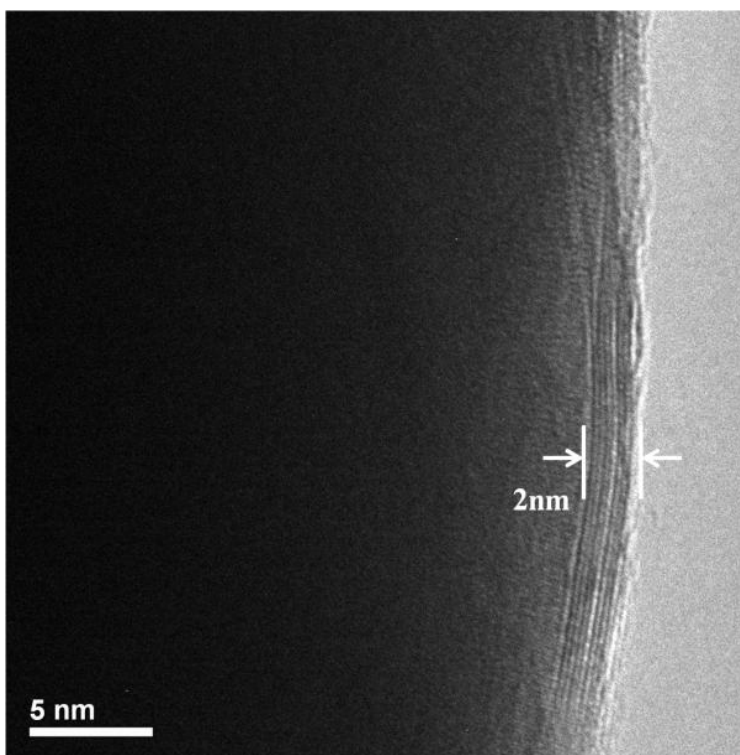
(a) hollow carbon



(b)  $\text{Cu}_5\text{Sn}_6@\text{void}@C$  yolk-shell



(c)  $\text{Cu}_5\text{Sn}_6$  alloy



(d)  $\text{Cu}_5\text{Sn}_6$  alloy (high resolution)

**Figure 4.** TEM images of the composite powder post-treated at 1000°C.

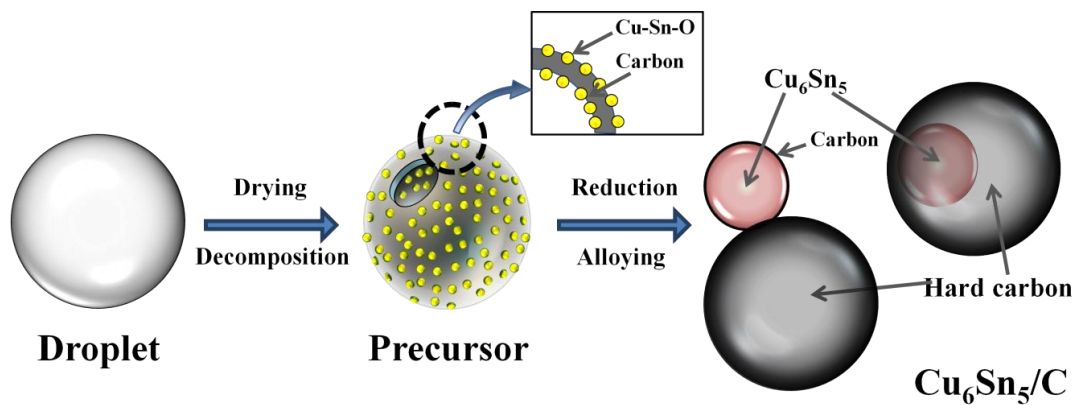
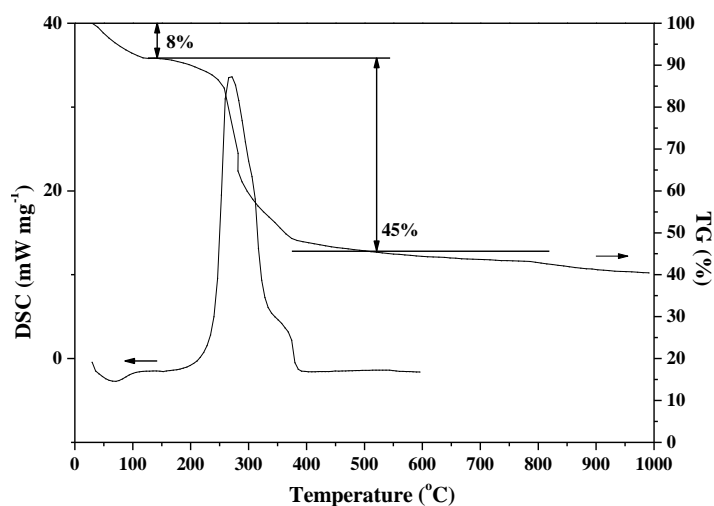
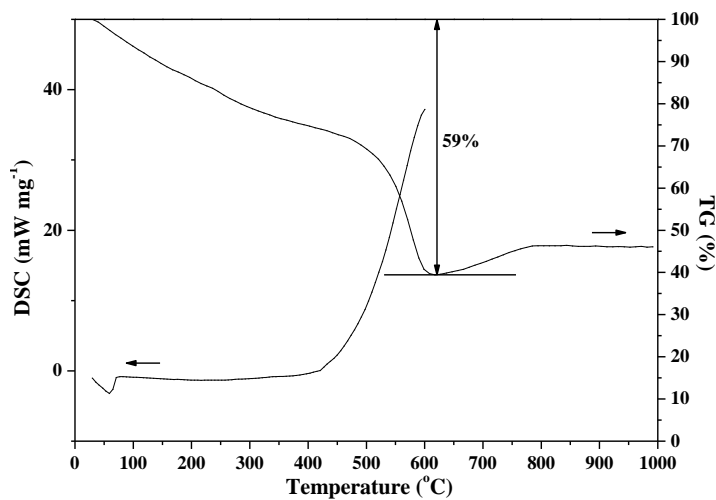


Figure 5. Formation mechanism of the alloy composite powders.



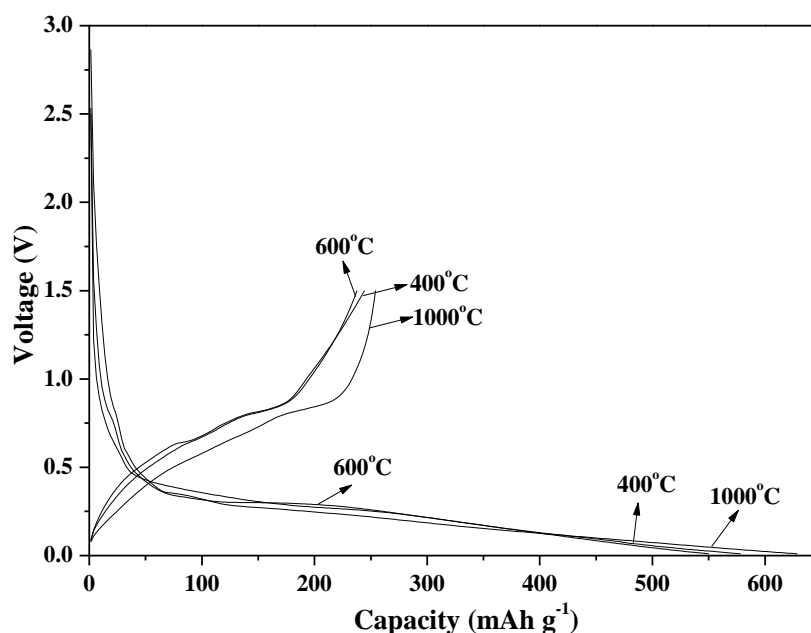
(a) precursor



(b) 1000°C

Figure 6. TG/DSC curves of the precursor and post-treated powders at 1000°C.

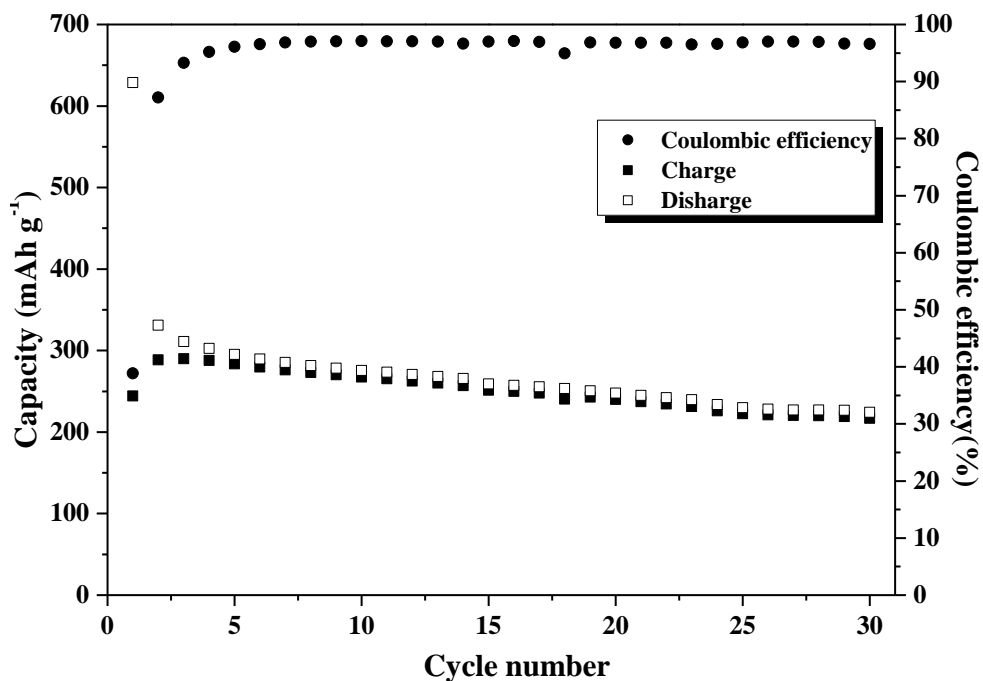
The others moved to the outside of the carbon powder particles. The composite powders thus contained a mixture of  $\text{Cu}_5\text{Sn}_6@ \text{void} @ \text{C}$  yolk-shell,  $\text{Cu}_5\text{Sn}_6$  alloy, and hollow carbon particles. Fig. 4 shows the TEM images of the  $\text{Cu}_5\text{Sn}_6@ \text{void} @ \text{C}$  yolk-shell,  $\text{Cu}_5\text{Sn}_6$  alloy, and hollow carbon powder particles. In the yolk-shell powders, mobile  $\text{Cu}_5\text{Sn}_6$  powder particles are located inside the hollow carbon powder particles. The mean sizes of the  $\text{Cu}_5\text{Sn}_6$  alloy and carbon powder particles, as shown in Figs. 4 (b) and (c), are 0.7 and 1.6  $\mu\text{m}$ , respectively. The thickness of the carbon shell, as measured from the TEM image shown in Fig. 4 (a), was 50 nm. The submicron  $\text{Cu}_5\text{Sn}_6$  alloy powder particles were coated with a thin carbon layer, as shown in the HR-TEM image in Fig. 4 (d).



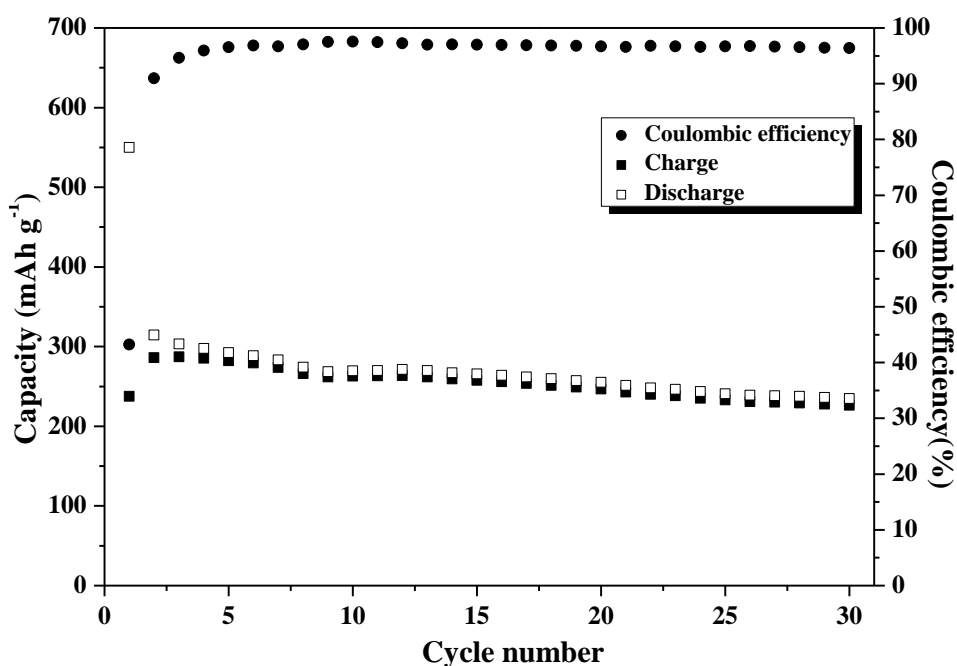
**Figure 7.** Initial charge/discharge curves of the powders post-treated at various temperatures.

Fig. 6 shows the TGA/DSC curves for the precursor and the reduced composite powders measured in air. The TGA curve for the precursor powders indicates two weight losses at temperatures below 1000°C. The first prominent weight loss region from 40 to 130°C resulted from the loss of adsorbed water. The high amount of weight loss in the region 200 to 500°C in the TGA curve for the precursor powders can be attributed to the decomposition of the carbon material. The total weight loss of the precursor powders due to the decomposition of the carbon material was 45%. The composite powders reduced at 1000°C also exhibited high total weight loss of 59% due to both the loss of adsorbed water and the decomposition of the carbon material. The main exothermic peaks associated with the decomposition of the carbon materials in the precursor and the reduced composite powders were located at ~270 and above 600°C, respectively, in the DSC curves. The high reduction temperature of 1000°C transformed the soft carbon in the precursor powders into hard carbon. The slight increase in the weight of the reduced composite powders was due to the oxidation of the alloy powders above 600°C.

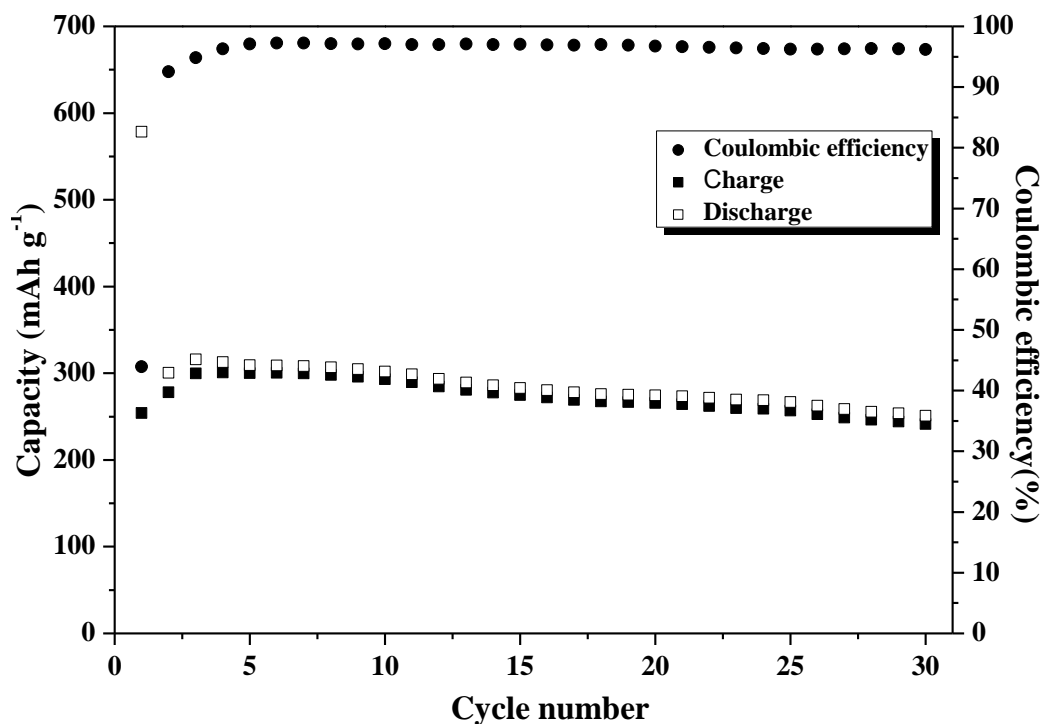
Fig. 7 shows the charge/discharge curves measured at room temperature at a constant current density of  $300 \text{ mA g}^{-1}$  in the range 0.01–1.5 V for the Cu-Sn-C composite powders reduced at various temperatures. The shapes of the initial charge and discharge curves were similar for all reduction temperatures. The initial discharge curves exhibited two discharge plateaus at  $\sim 0.3$  and near 0.0 V for all reduction temperatures.



(a) 400°C



(b) 600°C



(c) 1000°C

**Figure 8.** Cycle properties and Coulombic efficiencies of the composite powders post-treated at various temperatures.

As is well-known from previous reports, the potential plateaus are attributed to the transformation of  $\text{Cu}_6\text{Sn}_5$  into  $\text{Li}_x\text{Sn}$  through a  $\text{Li}_2\text{CuSn}$  intermediate [18]. The charge curves also exhibited two charge plateaus at  $\sim 0.5$  and  $0.75$  V for all reduction temperatures. The shapes of the charge and discharge curves (data not shown) remained almost constant during cycling, indicating that the  $\text{Cu}_6\text{Sn}_5$  alloy electrode can be stably transformed between  $\text{Li}_x\text{Sn}$  and  $\text{Cu}_6\text{Sn}_5$  [18]. The initial discharge capacities of the composite powder electrodes reduced at 400, 600, and 1000°C were 628, 550, and 578  $\text{mAh g}^{-1}$ , respectively. The initial charge capacities of the composite powder electrodes reduced at 400, 600, and 1000°C were 244, 237, and 254  $\text{mAh g}^{-1}$ , respectively. The electrodes produced using the Cu-Sn-C composite powders with low active Cu-Sn alloy contents exhibited high initial charge/discharge capacities, even at a high current density of  $300 \text{ mA g}^{-1}$ . The composite powders exhibited low initial Coulombic efficiencies for all reduction temperatures. Hard carbons exhibit a lower Coulombic efficiency than graphite [35]. The irreversible capacity of hard carbons during the first cycle is attributed to solid electrolyte interface formation [36,37]. The Cu-Sn-C composite powders exhibited high hard-carbon content, as shown in Fig. 4 (a).

Fig. 8 shows the cycle performances and Coulombic efficiencies measured at room temperature at a constant current density of  $300 \text{ mA g}^{-1}$  in the range 0.01–1.5 V for electrodes produced using the composite powders reduced at various temperatures. The initial Coulombic efficiencies of electrodes produced using the composite powders reduced at 400, 600, and 1000°C were 38.8%, 43.2%, and 44%, respectively. During subsequent cycles, the electrodes exhibited high Coulombic efficiencies of

~98% for all reduction temperatures, indicating the high lithiation/delithiation reversibility in the composite powders. The charge capacities of the electrodes produced using the composite powders slightly increased with increasing number of cycles during the first three cycles for all reduction temperatures. The Cu-Sn alloy powder particles were several hundred nanometers in diameter. Therefore, the deep interior of the alloy powder particles was gradually activated within the first three cycles. The maximum charge capacities of the electrodes produced using the composite powders reduced at 400, 600, and 1000°C were 289, 285, and 300 mAh g<sup>-1</sup>, respectively. The charge capacities of the electrodes produced using the composite powders reduced at 400, 600, and 1000°C were 216, 226, and 241 mAh g<sup>-1</sup>, respectively, after 30 cycles, during which the capacity retentions were 75%, 79%, and 80%, respectively. The highly mixed Sn and Cu components and the phase homogeneities of the composite powders improved the initial charge/discharge capacities and the cycle properties of the electrodes, even at a high current rate of 300 mA g<sup>-1</sup>. The unique yolk-shell particle structure also improved the cycle properties of the electrodes produced using the composite powders. The hard-carbon shell prevented the aggregation and deactivation of the spherical Cu-Sn alloy powder particles existing inside and outside the shell during cycling. The flexible and thin carbon coating layer on the alloy powder particles also improved the stability of the electrodes produced using the composite powders during cycling. The electrodes produced using the composite powders reduced at 1000°C exhibited slightly higher capacities than did those produced using the composite powders reduced at 400 and 600°C. The phase homogeneity improved the electrochemical properties of the electrodes produced using the composite powders reduced at 1000°C.

#### 4. CONCLUSIONS

Hollow-structured SnO<sub>2</sub>-CuO-C composite powder particles are prepared using spray pyrolysis. Nanosized SnO<sub>2</sub>-CuO composite particles are uniformly dispersed over the inner and outer surfaces of the spherical carbon powder particles. Uniquely structured Cu<sub>6</sub>Sn<sub>5</sub>-C composite powder particles are obtained after reduction at 1000°C. Submicron Cu<sub>6</sub>Sn<sub>5</sub> alloy powder particles uniformly coated with a carbon layer are located either inside or outside the hollow hard-carbon powder particles, which exhibits a mean size of 1.6 μm. Peaks of negligible intensity associated with the Cu<sub>3</sub>Sn and Sn impurity phases are observed in the XRD patterns for the composite powders. The charge capacities of the electrodes produced using the composite powders reduced at 1000°C are 254, 300, and 241 mAh g<sup>-1</sup> during the 1<sup>st</sup>, 3<sup>rd</sup>, and 30<sup>th</sup> cycles, respectively. The inactive hard-carbon content is too high to obtain high charge capacity from the electrodes produced using the composite alloy powders. Optimizing the types of spray solution and the preparation conditions will improve the electrochemical properties of the composite alloy powders prepared using spray pyrolysis.

#### ACKNOWLEDGEMENT

This work was supported by the National Research Foundation of Korea(NRF) grant funded by the Korea government(MEST) (No. 2012R1A2A2A02046367). This study was supported by the

Converging Research Center Program through the National Research Foundation of Korea (NRF) funded by the Ministry of Education, Science and Technology (2011-50210).

## References

1. C.H. Tan, G.W. Qi, Y.P. Li, J. Guo, X. Wang, D.L. Kong, H.J. Wang, S.Y. Zhang, *Int. J. Electrochem. Sci.*, 7 (2012) 10303.
2. D. Larcher, L.Y. Besulien, D.D. MacNeil, J.R. Dahn, *J. Electrochem. Soc.*, 147 (2000) 1658.
3. M.G. Kim, S.J. Sim, J.P. Cho, *Adv. Mater.*, 22 (2010) 5154.
4. M. Lu, Y. Tian, Y. Li, W. Li, X. Zheng, B. Huang, *Int. J. Electrochem. Sci.*, 7 (2012) 760.
5. L.B. Wang, S. Kitamura, K. Obata, S. Tanase, T. Sakai, *J. Power Sources*, 141 (2005) 286.
6. M. Valvo, U. Lafont, L. Simonin, E.M. Kelder, *J. Power Sources*, 174 (2000) 428.
7. J. Yang, Y. Takeda, Q. Li, N. Imanishi, O. Yamamoto, *J. Power Sources*, 90 (2000) 64.
8. F.S. Ke, L. Huang, H.H. Jiang, H.B. Wei, F.Z. Yang, S.G. Sun, *Electrochem. Commun.* 9 (2007) 228.
9. H. Mukaibo, T. Sumi, T. Yokoshima, T. Momma, T. Osaka, *Electrochem. Solid-State Lett.*, 6 (2003) A218.
10. G.X. Wang, L. Sun, D.H. Bradhurst, S.X. Dou, H.K. Liu, *J. Alloys Compd.*, 299 (2000) L12.
11. H. C. Shin, M. Liu, *Adv. Funct. Mater.*, 15 (2005) 582.
12. J. Wolfenstine, S. Campos, D. Foster, J. Read, W.K. Behl, *J. Power Sources*, 109 (2002) 230.
13. S. Gürmen, S. Stopić, B. Friedrich, *Mater. Res. Bull.*, 41 (2006) 1882.
14. D.G. Kim, H. Kim, H.J. Sohn, T. Kang, *J. Power Sources*, 104 (2002) 221.
15. S. Liu, Q. Li, Y. Chen, F. Zhang, *J. Alloys Compd.*, 478 (2009) 694.
16. W.J. Cui, F. Li, H.J. Liu, C.X. Wang, Y.Y. Xia, *J. Mater. Chem.*, 19 (2009) 7202.
17. S.H. Ju, H.C. Jang, Y.C. Kang, *J. Power Sources*, 189 (2009) 163.
18. X.Y. Fan, F.S. Ke, G.Z. Wei, L. Huang, S.G. Sun, *Electrochem. Solid-State Lett.*, 11 (2008) A195.
19. N. Jayaprakash, N. Kalaiselvi, C.H. Doh, *J. Appl. Electrochem.*, 37 (2007) 567.
20. R. Zheng, X. Meng, F. Tang, L. Zhang, J. Ren, *J. Phys. Chem. C*, 113 (2009) 13065.
21. K. Wang, X. He, L. Wang, J. Ren, C. Jiang, C. Wan, *J. Electrochem. Soc.*, 10 (2006) A1859.
22. K. Wang, X. He, L. Wang, J. Ren, C. Jiang, C. Wan, *Solid State Ionics*, 178 (2007) 115.
23. J.G. Ren, X.M. He, K. Wang, W.H. Pu, *Ionics*, 16 (2010) 503.
24. W.M. Zhang, J.S. Hu, Y.G. Guo, S.F. Zheng, L.S. Zhong, W.G. Song, L.J. Wan, *Adv. Mater.*, 20 (2008) 1160.
25. X.J. Wu, D. Xu, *Adv. Mater.*, 22 (2010) 1516.
26. K. Kamata, Y. Lu, Y. Xia, *J. Am. Chem. Soc.*, 125 (2003) 2384.
27. M.S. Kim, K.N. Sohn, H.B. Na, T.H. Hyeon, *Nano Lett.*, 2 (2002) 1383.
28. Y.G. Sun, B. Wiley, Z.Y. Li, Y.N. Xia, *J. Am. Chem. Soc.*, 126 (2003) 9399.
29. J. Lee, J.C. Park, H. Song, *Adv. Mater.*, 20 (2008) 1523.
30. X.W. Lou, Y. Wang, C. Yuan, J.Y. Lee, L.A. Archer, *Adv. Mater.*, 18 (2006) 2325.
31. T. Zhang, J. Ge, Y. Hu, Z. Qiao, S. Aloni, Y.D. Yin, *Angew. Chem. Int. Ed.*, 47 (2008) 5806.
32. D.M. Cheng, X.D. Zhou, H.B. Xia, H.S.O. Chan, *Chem. Mater.*, 17 (2005) 3578.
33. S.H. Ju, H.C. Jang, Y.C. Kang, D.W. Kim, *J. Alloys Compd.*, 478 (2009) 177.
34. H.C. Jang, S.H. Ju, Y.C. Kang, *J. Alloys Compd.*, 478 (2009) 206.
35. W. Guoping, Z. Bolan, Y. Min, X. Xiaoluo, Q. Meizheng, Y. Zuolong, *Solid State Ionics*, 176 (2005) 905.
36. F. Béguin, F. Chevallier, C. Vix-Guterl, S. Saadallah, V. Bertagna, J.N. Rouzaud, E. Frackowiak, *Carbon*, 43 (2005) 2160.
37. E. Buiel, J.R. Dahn, *Electrochim. Acta*, 45 (1999) 121.